
COMPARATIVE STUDY OF KONDO EFFECT IN VANADIUM DICHALCOGENIDES VX_2 ($X=Se$ & Te)

A PREPRINT

✉ **Indrani Kar**

Department of Condensed Matter and Materials Physics
S. N. Bose National Centre for Basic Sciences
Salt Lake, JD Block, Sector III, Bidhannagar, Kolkata-700106, India

✉ **Susanta Ghosh**

Department of Condensed Matter and Materials Physics
S. N. Bose National Centre for Basic Sciences
Salt Lake, JD Block, Sector III, Bidhannagar, Kolkata-700106, India

✉ **Shuvankar Gupta**

Condensed Matter Physics Division,
Saha Institute of Nuclear Physics
A CI of Homi Bhabha National Institute
1/AF, Bidhannagar, Kolkata-700064, India

✉ **Sudip Chakraborty**

Condensed Matter Physics Division,
Saha Institute of Nuclear Physics
A CI of Homi Bhabha National Institute
1/AF, Bidhannagar, Kolkata-700064, India

✉ **S. Thirupathaiah***

Department of Condensed Matter and Materials Physics
S. N. Bose National Centre for Basic Sciences
Salt Lake, JD Block, Sector III, Bidhannagar, Kolkata-700106, India
setti@bose.res.in

December 18, 2023

ABSTRACT

We report on the electrical transport, magnetotransport, and magnetic properties studies on the transition metal dichalcogenides VSe_2 and VTe_2 and draw a comprehensive comparison between them. We observe Kondo effect in both systems induced by the exchange interaction between localized moments and conduction electrons at low temperature, resulting into resistance upturn at 6 K for VSe_2 and 17 K for VTe_2 . From the field dependent resistance measurements we find that the data is fitted best with modified Hamann equation corrected by the quantum Brillouin function for VSe_2 , while the data is fitted best with modified Hamann equation corrected by the classical Langevin function for VTe_2 . Interestingly, we observe a contrasting magnetoresistance (MR) property between these systems across the Kondo temperature. That means, negative MR is found in both systems in the Kondo state. In the normal state MR is positive for VSe_2 , while it is negligible for VTe_2 . In addition, both systems show weak ferromagnetism at low temperature due to intercalated V atoms.

Keywords Transition metal dichalcogenides · Single crystal · Kondo effect · Hamann Equation · Brillouin function · Langevin function

1 Introduction

For more than six decades, the TMDCs are widely discussed in the verge of the ground state properties like CDW and superconductivity [1–9]. Among them, from the group V TMDCs, the ditelluride-based compounds are isostructural to each other having the monoclinic crystal structure with $1T'$ phase below 300 K [10–15], while the diselenide- and the disulfur-based compounds are available in the trigonal crystal structure with $1T$ or $2H$ phase [16–21]. Despite being isostructural, these compounds show differing electronic and magnetic properties. For instance, VTe_2 shows a normal to commensurate CDW (C-CDW) transition at 474 K [13, 22, 23], while $NbTe_2$ shows incommensurate CDW (IC-CDW) transition at 550 K and IC-CDW to C-CDW transition at room temperature [11, 24], in addition to a superconducting transition (T_c) at ≈ 0.5 K [25, 26]. On the other hand, $TaTe_2$ shows a normal to IC-CDW transition at 170 K [27–29]. Similarly, VSe_2 shows an IC-CDW transition at around 110 K and an IC-CDW to C-CDW at 70 K [30–33]. $NbSe_2$ shows an IC-CDW transition at 33 K and superconductivity at 7.2 K [34]. $TaSe_2$ shows an IC-CDW transition at 600 K and a C-CDW transition at 473 K in the $1T$ phase [35], while an IC-CDW transition at 122 K and a C-CDW transition at 90 K is found in the $2H$ phase [16, 36]. VS_2 is reported to show a CDW transition below 304 K [21, 37, 38]. Though NbS_2 is not found to show a clear CDW order, recently it was suggested to be at the verge of a CDW order following the diverse electronic properties in NbS_2 [20, 39]. On the other hand, TaS_2 shows IC-CDW phase below 550 K and a nearly commensurate CDW (NC-CDW) phase below 350 K and C-CDW phase was found below 180 K in the $1T$ phase [40], while a short range CDW transition is found below 75 K in the $2H$ phase [41]. Magnetotransport studies on $TaTe_2$ and $NbTe_2$ suggest a linear dependence of MR on the applied field [11, 27], while a quadratic MR is found from VTe_2 [42]. In contrast to $TaTe_2$ and $NbTe_2$, VTe_2 shows a weak ferromagnetic ordering at low temperature. Also, VTe_2 is found to show a resistivity upturn due to Kondo effect [33, 42–44]. However, the resistivity upturn found in VSe_2 is still under debate. Some reports interpreted the resistivity upturn to the Kondo effect in the paramagnetic regime [43], while the other reports interpreted it to a weak localization [42]. $TaSe_2$ in $2H$ phase is reported to show antiferromagnetic ordering [45]. TaS_2 in the $1T$ phase shows ferromagnetic ordering due to localized spins [46]. As a matter of fact, Kondo effect was not observed in $TaTe_2$ and $NbTe_2$ systems.

In this contribution, we report a comprehensive comparison study between VSe_2 and its isovalent compound VTe_2 on their electrical transport, magnetotransport, and magnetic properties. We observe a low temperature resistivity upturn in both systems due to Kondo effect induced by the exchange interaction between localized moments and conduction electrons at low temperature. The electrical transport data of VSe_2 measured under various applied magnetic fields can be explained well with the modified Hamann equation following the Brillouin function [47] using the quantum mechanical behaviour of magnetic moments [48]. From a similar transport study on VTe_2 we find that the data can be fitted well with modified Hamann equation following the Langevin function [42] using the classical theory [48]. Foremost these observations confirm the presence of Kondo effect in both systems, specifically for VSe_2 in which the mechanism of resistivity upturn is elusive [33, 42, 43]. Further, we find negative magnetoresistance (MR) from both systems in the Kondo state, while MR behaves differently in the normal state.

2 Experimental Details

Single crystal of VTe_2 was grown by the chemical vapor transport (CVT) technique using iodine (crystalline, 99.99%, metals basis, Alfa Aesar) (2 mg/cm^3) as a transport agent [49]. In the first step, stoichiometric amounts of V (powder, 99.5%, metals basis, Alfa Aesar) and Te (powder, 99.99%, metals basis, Alfa Aesar) were mixed thoroughly and sealed in a quartz ampoule under vacuum. The ampoule was then slowly heated to 1000°C at a rate of 2.5°C/min and kept there for 8 h before quenched in the normal water. The powder was regrinded, sealed in quartz ampoule under vacuum together with pieces of crystallized iodine (crystalline, 99.99%, metals basis, Alfa Aesar) (2 mg/cm^3). The ampoule was loaded into a three-zone tube furnace where the temperatures were set at 900°C at the hot-zone and 810°C was set at the cold-zone. After 5 days of reaction, we obtained shiny single crystals with a typical dimension of $5 \text{ mm} \times 5 \text{ mm}$ at the cold-zone. Similarly, single crystals of VSe_2 were grown by the above method by mixing the stoichiometric amounts of V (powder, 99.5%, metals basis, Alfa Aesar) and Se (shot, 99.999%, metals basis, Alfa Aesar), except that 1000°C was set at the hot-zone and 950°C was set at the cold-zone. After 5 days of reaction, we obtained shiny single crystals of typical dimension $15 \text{ mm} \times 6 \text{ mm}$ at the cold-zone.

Chemical composition of the single crystals were determined by the energy-dispersive X-ray analysis (EDX) equipped with a scanning electron microscope (Quanta 250 FEG) and phase purity was checked by X-ray diffraction (XRD) patterns measured using $\text{Cu-}k_\alpha$ -radiation (Rigaku MiniFlex II and Rigaku SmartLab 9KW). Differential scanning calorimetry (DSC) (Q2000 of TA Instruments) was performed to measure the heat flow curve of the sample in both heating and cooling modes.

Electrical transport measurements were done in a physical property measurement system (Quantum Design PPMS-9T) using a standard four-probe method, with the electrical current applied along the plane of sample (*ab*-plane). For

magnetotransport measurements the magnetic field was applied at different polar angles with respect to the ab -plane. Copper (Cu) leads were connected to the sample by vacuum compatible silver epoxy Epo-Tek H2OE. The sample temperature was varied between 2 K and 330 K during the transport measurements. DC magnetization measurements were performed using the magnetic property measurement system (Quantum Design MPMS-7T) equipped with vibrating sample magnetometer superconducting quantum interference device (VSM-SQUID). Temperature dependence of the magnetization in zero-field-cooled (ZFC) and field-cooled (FC) modes has been carried out under different applied magnetic fields up to 7 T in the temperature range of 5-300 K. Field dependent magnetization [$M(H)$] has also been carried out at different temperatures.

3 Results and Discussions

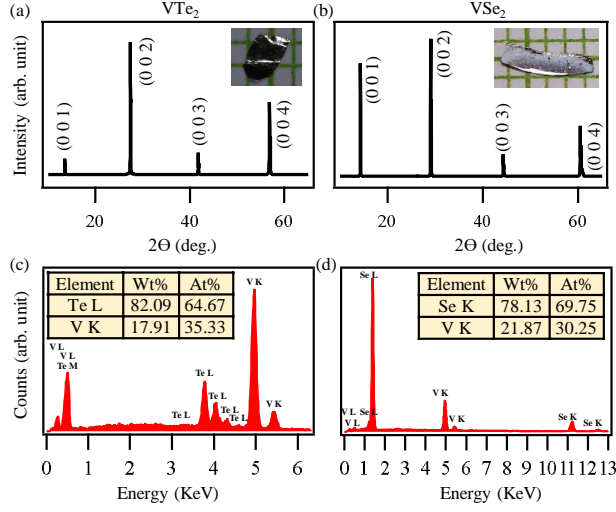


Figure 1: (a) and (b) Powder X-ray diffraction (XRD) pattern of VTe_2 and VSe_2 single crystals. Insets in (a) and (b) are the optical images of the single crystals. (c) and (d) Energy dispersive X-ray spectroscopy (EDX) data of VTe_2 and VSe_2 single crystals, respectively.

Single crystals of VTe_2 and VSe_2 were structurally analyzed using the powder X-ray diffraction (XRD) at room temperature. High intense diffraction peaks corresponding to the (001) plane of VTe_2 are shown in Fig. 1(a) and (001) plane of VSe_2 are shown in Fig. 1(b). VTe_2 crystallizes into the monoclinic structure with the space group $C2/m$ (12) in the $1T'$ phase at room temperature, while VSe_2 crystallizes into the trigonal structure with space group of $P\bar{3}m1$ (164) in the $1T$ phase [13, 50]. From EDX measurements as shown in Figs. 1(c) and 1(d) we identify that the studied samples have actual compositions of $V_{1.08}Te_2$ and $V_{0.86}Se_2$, respectively. Thus, we obtained 8% vanadium excess VTe_2 and 14% vanadium deficient VSe_2 single crystals. Herein, for the convenience, we represent these crystals by their nominal compositions of VSe_2 and VTe_2 .

Fig. 2(a) shows temperature dependent in-plane electrical resistance of VTe_2 . The resistance curve shows a metallic nature, in principle, except that an upturn is noticed at low temperature with a resistance minima at $T_m=17$ K as can be seen from the inset of Fig. 2(a). To explore further on the resistance upturn mechanism, it was measured at various magnetic fields within the temperature range of 2-40 K as plotted in Fig. 2(b). We observe decrease in resistance upturn with increasing magnetic field of up to 9 T. Further, the field dependent resistance curves are perfectly fitted with the Eq. 1 and Eq. 2 without and with applied magnetic field, respectively. In Eq. 1, the first term (R_0) is residual resistance, the second term (qT^2) represents the electron-electron interaction, and the third term is the Hamann expression [51] due to $s-d$ exchange interaction [42, 52]. Hamann expression is an empirical equation used to calculate the exchange interaction between localized magnetic moments and conduction electrons. In the third term, R_{KO} is the temperature-independent Kondo resistance, T_K is the Kondo temperature, and S is the total spin of the magnetic impurities. $T_{eff} = \sqrt{T^2 + T_W^2}$, where $k_B T_W$ is the effective Ruderman-Kittel-Kasuya-Yosida (RKKY) interaction strength. From the fitting, we obtained a Kondo temperature $T_K=12$ K and $S=0.5$. These values are in good agreement with previous report on VTe_2 single crystal [42]. In Eq. 2, the Hamann term is multiplied by $[1 - L^2(\frac{\mu H}{k_B T_{eff}})]$ where $L(x)$ is Langevin function $L(x) = \coth(x) - 1/x$ (see Table 1 for the fitting parameters). Primarily, Hamann equation involves Brillouin function [47] to describe the quantum mechanical behavior of the magnetic moments and provides a more accurate description of their statistical distribution. In quantum theory, the magnetic moments are quantized and

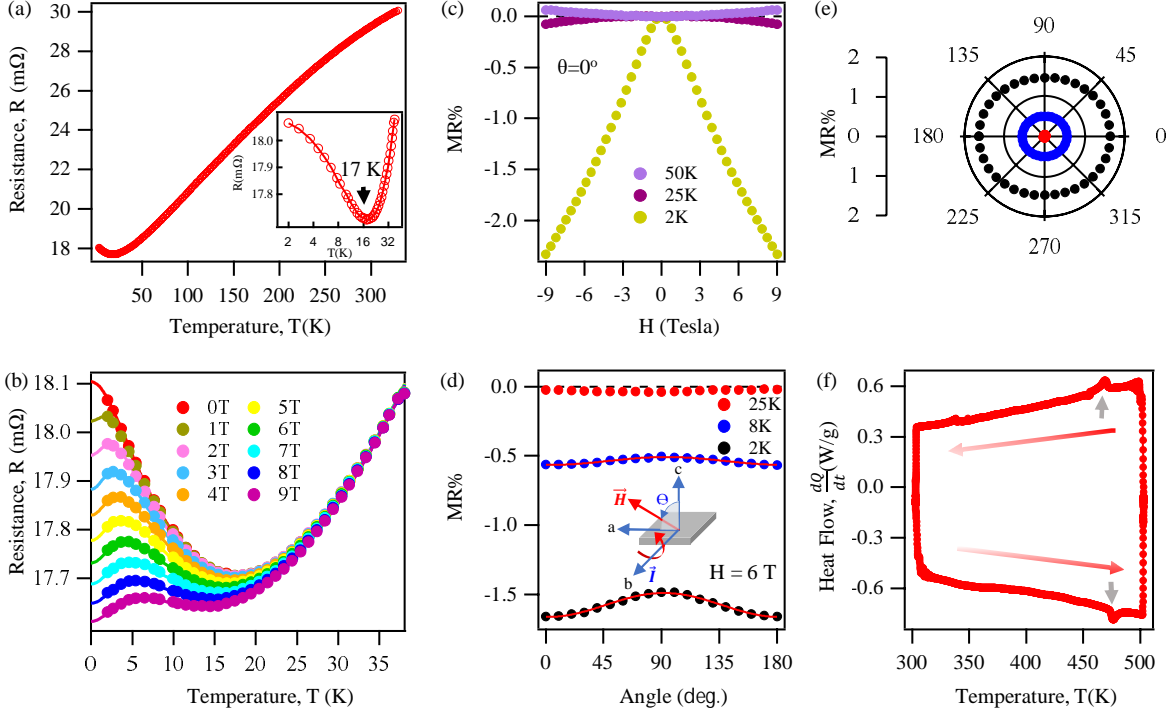


Figure 2: (a) In-plane electrical resistance of VTe_2 plotted as a function of temperature. Inset in (a) shows low-temperature resistance upturn at a temperature minima $T_m=17$ K. (b) Temperature dependent electrical resistance plotted for various applied magnetic fields parallel to c -axis. Solid lines in (b) are fittings to Eq. 1 and Eq. 2. (c) Magnetoresistance, MR (%), plotted as a function of field applied parallel to the c -axis ($\theta = 0^\circ$). (d) MR (%) plotted as function of applied field angle. Measuring geometry is shown in the inset of (d). (e) Symmetrized MR (%) of (d) is plotted in the polar graph. (f) Differential scanning calorimetry (DSC) data is plotted as function of temperature for both cooling and heating cycle. In (f), the charge density wave ordering temperature (T_{CDW}) is marked from both heating and cooling cycles.

the orientations of magnetic moment with respect to applied magnetic field are specified by some possible components of magnetic moment along field direction [48]. On the other hand, the Langevin function [42] is a simplified model derived from classical statistical mechanics. In Langevin's classical theory, it is assumed that the mutual interaction between the magnetic dipoles is negligible and magnetic moments can possess any orientation with respect to applied magnetic field [48].

$$R(T) = R_0 + qT^2 + R_{KO} \left[1 - \frac{\ln\left(\frac{T_{eff}}{T_K}\right)}{\sqrt{\ln^2\left(\frac{T_{eff}}{T_K}\right) + S(S+1)\pi^2}} \right] \quad (1)$$

$$R(T) = R_0 + qT^2 + R_{KO} \left[1 - \frac{\ln\left(\frac{T_{eff}}{T_K}\right)}{\sqrt{\ln^2\left(\frac{T_{eff}}{T_K}\right) + S(S+1)\pi^2}} \right] \left[1 - L^2\left(\frac{\mu H}{k_B T_{eff}}\right) \right] \quad (2)$$

Fig. 2(c) depicts magnetoresistance (MR%), $MR\% = \frac{R(H)-R(0)}{R(0)} \times 100$, plotted as a function of applied field measured at below (2 K) and above (25 K & 50 K) the Kondo temperatures. We notice that at 2 K, below the Kondo temperature, VTe_2 shows a negative MR and above Kondo temperature, the MR is negligible. This is because the magnetic field reduces fluctuations of localized impurity magnetic moments and spin dependent exchange scattering [53]. Hence, below a critical magnetic field (B_c), the MR is negative and above B_c , the Kondo effect vanishes. In case of VTe_2 the

H (T)	R_0 ($m\Omega$)	q ($\mu\Omega/K^2$)	R_{KO} ($m\Omega$)	T_W (K)	μ (μ_B)
0	16.6140(4)	0.5719(4)	1.0782(4)	3.900(3)	
1	16.6530(4)	0.5645(4)	1.0316(4)	2.423(3)	4.042(3)
2	16.6563(4)	0.5641(4)	1.0295(4)	2.665(3)	2.569(3)
3	16.6786(4)	0.5596(4)	1.0028(4)	2.823(3)	2.045(3)
4	16.7015(4)	0.5561(4)	0.9740(4)	3.147(3)	1.789(3)
5	16.7343(4)	0.5508(4)	0.9331(4)	3.396(3)	1.631(3)
6	16.7778(4)	0.5435(4)	0.8780(4)	3.632(3)	1.510(3)
7	16.8104(4)	0.5398(4)	0.8334(4)	3.916(3)	1.445(3)
8	16.8592(4)	0.5320(4)	0.7692(4)	4.135(3)	1.379(3)
9	16.9061(4)	0.5263(4)	0.7054(4)	4.332(3)	1.329(3)

Table 1: Kondo fitting parameters of VTe_2

value of B_c is very high [42] which is beyond our experimental scope. Fig. 2(d) shows MR (%) plotted as a function of field angle with respect to the sample surface normal (c -axis) at an applied field of 6 T. Measuring geometry is shown in the inset of Fig. 2(d). Red solid-lines in Fig. 2(d) are fittings to the Eq. 3. In Eq. 3, the first term is a constant and α is an amplitude. Fig. 2 (e) shows symmetrized angular dependent MR plotted in the polar graph for the temperatures 2 K, 8 K, and 50 K. As can be seen from Fig. 2 (e), MR shows in-plane small anisotropy in the Kondo state (2 K) but becomes completely isotropic in the normal state (8 and 50 K). Ideally Kondo systems show isotropic MR but a small anisotropy could be there due to the presence of a crystal anisotropy [53]. DSC measurements are performed in both heating and cooling modes with a ramp rate of $dT/dt=10$ K/min as depicted in Fig. 2(f). During cooling and heating cycles of DSC measurements we noticed a hump and a dip, respectively, at a sample temperature of 470 ± 5 K that is originated from the charge density wave (CDW) [22].

$$MR(\theta) = MR_0 + \alpha \cos(2\theta) \quad (3)$$

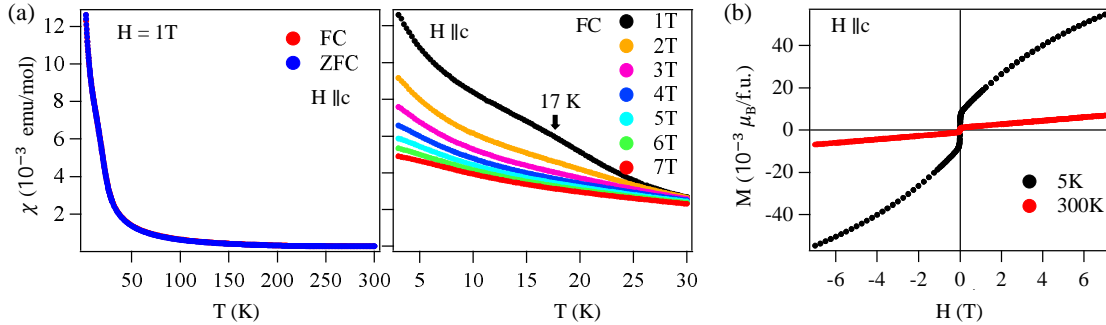


Figure 3: (a) Magnetic susceptibility of VTe_2 plotted as a function of temperature with a field of 1 T applied parallel to c -axis measured in the FC and ZFC modes. (b) Same as (a) but measured for different magnetic fields in the FC mode. (c) Magnetization isotherms $M(H)$ measured at 5 K and 300 K.

Fig. 3 shows magnetic measurements on VTe_2 with field applied parallel to the c -axis. Fig. 3(a) shows temperature dependent magnetic susceptibility measured with a field of 1 T within the temperature range of 3-300 K in the field-cooled (FC) and zero-field-cooled (ZFC) modes. Here, it can be seen that ZFC and FC are identical. Further, we measured the temperature dependent magnetic susceptibility by varying the field in the FC mode as shown in Fig. 3(b). A broad hump-like structure with a maximum at around 17 K has been noticed in the susceptibility data when measured with a magnetic field of 1 T, which is then eventually disappears above 3 T as we increase the field due to the crossover from high temperature localized moments of Kondo impurities to fully compensated moments at low temperature [42, 54]. However, at higher magnetic fields this crossover gets weaker as a result the resistance upturn decreases. Fig. 3(c) shows magnetization isotherms, $M(H)$, measured at 5 and 300 K. From the $M(H)$ data we notice a soft ferromagnetic-like ordering at the room temperature which is in agreement with previous reports on VTe_2 [47, 55, 56].

Next, Fig. 4(a) shows temperature dependent zero-field in-plane electrical resistance of VSe_2 . Overall, the resistance curve suggests a metallic behaviour except that a hump at around 100 K and a resistance upturn at low temperature

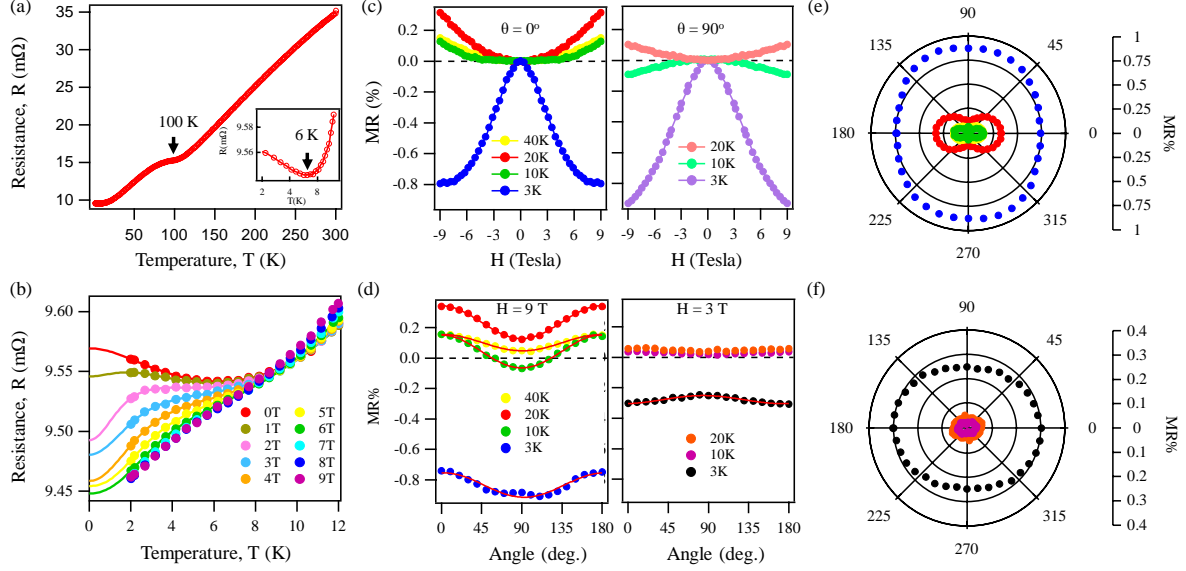


Figure 4: (a) In-plane electrical resistance of VSe_2 plotted as a function of temperature. A hump at CDW transition temperature of 100 K is noticed on the resistance curve. Inset in (a) shows the resistance upturn at a temperature minima $T_m=6$ K. (b) Temperature dependent electrical resistance plotted for various magnetic fields applied parallel to the c -axis. Solid lines in (b) are fittings to Eq. 4 and Eq. 5. (c) Magnetoresistance, MR (%) plotted as a function of field applied parallel to the c -axis ($\theta = 0^\circ$) is in the left panel and for the field applied perpendicular to the c -axis ($\theta = 90^\circ$) is shown in the right panel. (d) MR (%) is plotted as function of the field angle with applied field of 9 T (left panel) and 3 T (right panel). (e) Symmetrized MR (%) of (d) is plotted in the polar graph with an applied field of 9 T. (f) Symmetrized MR (%) of (d) is plotted in the polar graph with an applied field of 3 T.

is observed. The hump at 100 K is due to the incommensurate charge density order (IC-CDW) as noticed in the previous reports from this system [30, 33, 43, 44, 57–61]. Inset in Fig. 4(a) shows a resistance minima (T_m) at 6 K. To understand the resistance upturn mechanism, we performed field dependent resistance measurements within the temperature range of 2 K to 12 K by varying the magnetic fields up to 9 T as plotted in Fig. 4(b). As can be seen from Fig. 4(b), resistance upturn decreases with increasing field and disappears at 7 T, suggesting Kondo effect as the possible origin of the resistance upturn. Solid-lines in Fig. 4(b) are the fittings to Eq. 4 in absence of applied magnetic field and Eq. 5 in presence of applied magnetic field with a modified Hamann term [43, 44, 47, 62]. Eq. 4 is almost similar to Eq. 1, except that the second term (qT^3) in Eq. 4 represents the interband ($s-d$) $e-ph$ scattering while it is $e-e$ scattering (qT^2) contribution in Eq. 1. From the fitting, we estimated a Kondo temperature (T_K) of about 6 K and the spin component $S=0.5$, which are in good agreement with previous report on VSe_2 [43]. In Eq. 5, the Hamann expression is modified using the Brillouin function, $B(x) = (\frac{2S+1}{2S}) \coth \frac{2S+1}{2S} x - \frac{1}{2S} \coth \frac{1}{2S} x$ in the quantum limit. See Table 2 for the fitting parameters.

$$R(T) = R_0 + qT^3 + R_{KO} \left[1 - \frac{\ln\left(\frac{T_{eff}}{T_K}\right)}{\sqrt{\ln^2\left(\frac{T_{eff}}{T_K}\right) + S(S+1)\pi^2}} \right] \quad (4)$$

$$R(T) = R_0 + qT^3 + R_{KO} \left[1 - \frac{\ln\left(\frac{T_{eff}}{T_K}\right)}{\sqrt{\ln^2\left(\frac{T_{eff}}{T_K}\right) + S(S+1)\pi^2}} \right] \left[1 - B^2\left(\frac{g\mu_B SH}{k_B T_{eff}}\right) \right] \quad (5)$$

Left panel in Fig. 4(c) depicts the field dependent MR(%), measured at various temperatures for the field applied parallel to c -axis ($\theta = 0^\circ$). The right panel in Fig. 4(c) depicts MR(%) measured perpendicular to c -axis ($\theta = 90^\circ$). We can see from Fig. 4(c) that for both field orientations the MR is negative (positive) below (above) the Kondo temperature (6 K). Fig. 4(d) depicts the angle dependent MR(%) measured at various temperatures with a magnetic field of 9 T (left panel) and 3 T (right panel). From Fig. 4(d) we can see that the MR(%) has a maximum for $H \parallel c$ and minimum for $H \perp c$ under

the magnetic field of 9 T. On the other hand it is reversed when the applied field is 3 T, which means that the MR(%) is minimum for $H \parallel c$ and maximum for $H \perp c$. Nevertheless, MR (%) sinusoidally depends on the field angle in going from $H \parallel c$ to $H \perp c$. The Red solid lines are the fits to Eq. 3. Figs. 4 (e) and 4 (f) represents the polar maps of the symmetrized data shown left and right panels of Fig. 4 (d), respectively. Figs. 4 (e) and 4 (f) clearly show the out-of-plane anisotropic MR(%) in VSe_2 . Interestingly, the anisotropy is rotated by 90° between 3 T and 9 T. Anisotropic MR at 9 T is in good agreement with previous study [59]. Also, note here that the anisotropic MR is significant above the Kondo state, i.e. at higher magnetic fields (9 T) irrespective of the temperature. In the Kondo state (3 T), a small anisotropic behaviour is observed which is negligible.

H (T)	R_0 ($m\Omega$)	q ($\mu\Omega/K^3$)	R_{KO} ($m\Omega$)	T_W (K)
0	9.4223(4)	0.0483(4)	0.1121(4)	2.455(3)
1	9.3600(4)	0.0485(4)	0.1751(4)	2.023(3)
2	9.4211(4)	0.0480(4)	0.1124(4)	1.452(3)
3	9.4017(4)	0.0497(4)	0.1367(4)	2.160(3)
4	9.4301(4)	0.0497(4)	0.1061(4)	1.832(3)
5	9.4508(4)	0.0480(4)	0.0843(4)	1.385(3)
6	9.4440(4)	0.0506(4)	0.0965(4)	1.694(3)

Table 2: Kondo fitting parameters of VSe_2

Figure 5 shows magnetic properties studies on the VSe_2 single crystals. Fig. 5(a) shows temperature dependent magnetic susceptibility measured with a magnetic field of 1 T applied parallel to the c -axis within the temperature range of 3-300 K in the ZFC and FC modes. Here, it can be seen that ZFC and FC are identical. To observe the effect of Kondo screening on the magnetic properties, we measured the susceptibility by varying the magnetic field of up to 7 T within the temperature range of 3-30 K in FC mode as shown in Fig. 5(b). Unlike in VTe_2 , we do not find a significant change in the susceptibility of VSe_2 as a function of applied field, probably due to the low Kondo temperature (6 K) found in VSe_2 . Fig. 5(b) shows the magnetization isotherm $M(H)$ measured at 5 and 300 K. We clearly notice a sigmoid like $M(H)$ curve at 5 K due to soft ferromagnetic ordering. This observation is different from previous reports where VSe_2 is found in bulk to be paramagnetic at all temperatures [60, 61, 63]. However, a strong ferromagnetic ordering is reported in monolayer VSe_2 grown on HOPG or MoS_2 substrate at the room temperature [63]. Another recent report also demonstrated a small ferromagnetic signal in stoichiometric bulk VSe_2 , which they suggest to arise from vanadium impurities intercalated between the van der Waals layers.

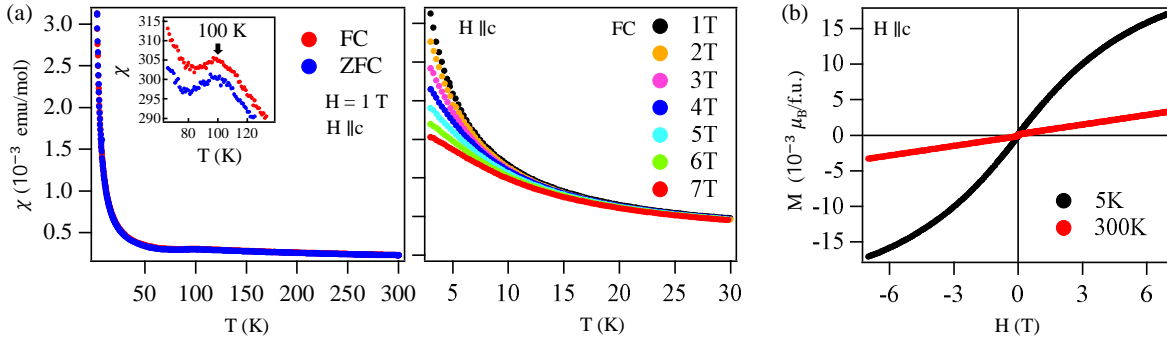


Figure 5: (a) Magnetic susceptibility of VSe_2 plotted as a function of temperature measured with a field of 1 T applied parallel to the c -axis in the FC and ZFC modes. (b) Same as (a) but measured for different magnetic fields in the FC mode. A hump in the magnetic susceptibility is noticed both in FC and ZFC modes at a CDW transition temperature of 100 K. (c) Magnetization isotherms $M(H)$ measured at 5 K and 300 K.

Finally, on comparing the electrical resistivity, magnetotransport, and magnetic properties between VTe_2 and VSe_2 , we find that both systems show low temperature resistivity upturn due to the Kondo effect with a Kondo temperature of 12 K for the former and 6 K for the later, suggesting stronger magnetic correlations in VTe_2 compared to VSe_2 . Both systems show negative MR in the Kondo state. VSe_2 shows negative to positive MR switching across the Kondo temperature of 6 K, while VTe_2 shows negligible MR above the Kondo temperature of 12 K. Moreover, above the Kondo state, a strong anisotropic MR is observed in the case of VSe_2 , while it is almost negligible in VTe_2 . In case of VTe_2 a weak anisotropic MR in the Kondo state is observed, whereas above the Kondo state the MR is negligible. Interestingly, though both systems show a low-temperature resistivity upturn due to the Kondo effect, under the magnetic field it

behaves differently for different compounds. That means, VTe_2 follows the Hamann law modified with the classical Langevin function with dominant contribution from the $e - e$ scattering, while VSe_2 follows the Hamann law modified with the quantum Brillouin function (see Eq. 5) with the dominant contribution from the interband ($s - d$) $e - ph$ scattering. Different functions applicable to the same Kondo effect observed in different compounds can be understood from their differing Kondo temperatures. That means, the Kondo temperature of VTe_2 (12 K) is almost two times higher than the Kondo temperature of VSe_2 (6 K). On the other hand, a previous study on the single-crystalline nanoplates of VTe_2 reported a Kondo temperature of 6 K and the resistivity data was best fitted following the Brillouin function [47]. These observations suggest that the Kondo temperature of these systems is thickness sensitive [64].

4 Conclusions

In conclusion, we have drawn a comprehensive comparison between the transition-metal dichalcogenides VSe_2 and VTe_2 on their electrical transport, magnetotransport, and magnetic properties. We observe the Kondo effect in both systems induced by the exchange interaction between localized moments and conduction electrons at low temperature, resulting into resistance upturn at Kondo temperature of 6 K for VSe_2 and 12 K for VTe_2 . From the field dependent resistance measurements we find that the data is fitted best with modified Hamann equation corrected by the quantum Brillouin function for VSe_2 , while the data is best fitted with modified Hamann equation corrected by the classical Langevin function for VTe_2 . Interestingly, we observe a contrasting magnetoresistance (MR) properties between these systems across the Kondo temperature. In both systems examined, there is a manifestation of weak ferromagnetism at low temperatures. This phenomenon can be attributed to the presence of intercalated V atoms in both systems.

5 Acknowledgements

S. T. greatly acknowledges the financial support given by SERB-DST through the Grant no. SRG/2020/00393. This research is made use of the Technical Research Centre (TRC) Instrument Facilities of S. N. Bose National Centre for Basic Sciences, established under the TRC project of Department of Science and Technology, Govt. of India. The authors thank Prof. Priya Mahadevan for fruitful discussions.

References

- [1] L. H. Brixner. Preparation and properties of the single crystalline AB_2 -type selenides and tellurides of niobium, tantalum, molybdenum and tungsten. *Journal of Inorganic and Nuclear Chemistry*, 24(3):257–263, 1962.
- [2] B. E. Brown. The crystal structures of $NbTe_2$ and $TaTe_2$. *Acta Crystallographica*, 20(2):264–267, feb 1966.
- [3] R. Nitsche, H. U. Bülsterli, and M. Lichtensteiger. Crystal growth by chemical transport reactions—I. *Journal of Physics and Chemistry of Solids*, 21(3-4):199–205, dec 1961.
- [4] J. A. Wilson and A. D. Yoffe. The transition metal dichalcogenides discussion and interpretation of the observed optical, electrical and structural properties. *Advances in Physics*, 18(73):193–335, may 1969.
- [5] J. A. Wilson, F. J. Di Salvo, and S. Mahajan. Charge-density waves and superlattices in the metallic layered transition metal dichalcogenides. *Advances in Physics*, 24(2):117–201, mar 1975.
- [6] S. Sharma, L. Nordström, and B. Johansson. Stabilization of charge-density waves in 1T- TaX_2 ($X=S, Se, Te$): First-principles total energy calculations. *Physical Review B*, 66(19), nov 2002.
- [7] Robert E. Thorne. Charge-Density-Wave Conductors. *Physics Today*, 49(5):42–47, may 1996.
- [8] C. M. WAYMAN and H. K. D. H. BHADSHIA. PHASE TRANSFORMATIONS, NONDIFFUSIVE. In *Physical Metallurgy*, pages 1507–1554. Elsevier, 1996.
- [9] Indrani Kar, Joydeep Chatterjee, Luminita Harnagea, Y. Kushnirenko, A. V. Fedorov, Deepika Shrivastava, B. Büchner, P. Mahadevan, and S. Thirupathiah. Metal-chalcogen bond-length induced electronic phase transition from semiconductor to topological semimetal in ZrX_2 ($X=Se$ and Te). *Physical Review B*, 101(16), apr 2020.
- [10] Kari Selte, Arne Kjekshus, H. Listou, Hertta Kyyhkynen, Ragnar A. Hoffman, and Anders Westerdahl. On the Magnetic Properties of Niobium Selenides and Tellurides. *Acta Chemica Scandinavica*, 19:258–260, 1965.
- [11] Hongxiang Chen, Zhilin Li, Xiao Fan, Liwei Guo, and Xiaolong Chen. Quantum linear magnetoresistance in $NbTe_2$. *Solid State Communications*, 275:16–20, jul 2018.
- [12] F. Clerc, C. Battaglia, H. Cercellier, C. Monney, H. Berger, L. Despont, M. G. Garnier, and P. Aebi. Fermi surface of layered compounds and bulk charge density wave systems. *Journal of Physics: Condensed Matter*, 19(35):355002, aug 2007.

- [13] K. D. Bronsema, G. W. Bus, and G. A. Wieggers. The crystal structure of vanadium ditelluride, $V_{(1+x)}Te_2$. *Journal of Solid State Chemistry*, 53(3):415–421, jul 1984.
- [14] Y. Liu, D. F. Shao, L. J. Li, W. J. Lu, X. D. Zhu, P. Tong, R. C. Xiao, L. S. Ling, C. Y. Xi, L. Pi, H. F. Tian, H. X. Yang, J. Q. Li, W. H. Song, X. B. Zhu, and Y. P. Sun. Nature of charge density waves and superconductivity in 1T-TaSe $_{2-x}$ Te $_x$. *Physical Review B*, 94(4), jul 2016.
- [15] T. Sörgel, J. Nuss, U. Wedig, R. K. Kremer, and M. Jansen. A new low temperature modification of TaTe $_2$ —Comparison to the room temperature and the hypothetical 1T-TaTe $_2$ modification. *Materials Research Bulletin*, 41(5):987–1000, may 2006.
- [16] Tomohisa Kumakura, Hiroki Tan, Tetsuya Handa, Masashi Morishita, and Hiroshi Fukuyama. Charge density waves and superconductivity in 2H-TaSe $_2$. *Czechoslovak Journal of Physics*, 46(S5):2611–2612, may 1996.
- [17] K. Terashima, T. Sato, H. Komatsu, T. Takahashi, N. Maeda, and K. Hayashi. Charge-density wave transition of 1T-VSe $_2$ studied by angle-resolved photoemission spectroscopy. *Physical Review B*, 68(15), oct 2003.
- [18] Gyeongcheol Gye, Eunseok Oh, and Han Woong Yeom. Topological Landscape of Competing Charge Density Waves in 2H-NbSe $_2$. *Physical Review Letters*, 122(1), jan 2019.
- [19] T. Ritschel, J. Trinckauf, K. Koepf, B. Büchner, M. v. Zimmermann, H. Berger, Y. I. Joe, P. Abbamonte, and J. Geck. Orbital textures and charge density waves in transition metal dichalcogenides. *Nature Physics*, 11(4):328–331, mar 2015.
- [20] Maxime Leroux, Laurent Cario, Alexei Bosak, and Pierre Rodière. Traces of charge density waves in NbS $_2$. *Physical Review B*, 97(19), may 2018.
- [21] M. Mulazzi, A. Chainani, N. Katayama, R. Eguchi, M. Matsunami, H. Ohashi, Y. Senba, M. Nohara, M. Uchida, H. Takagi, and S. Shin. Absence of nesting in the charge-density-wave system 1T-VS $_2$ as seen by photoelectron spectroscopy. *Physical Review B*, 82(7), aug 2010.
- [22] T. Ohtani, K. Hayashi, M. Nakahira, and H. Nozaki. Phase transition in $V_{1+x}Te_2$ ($0.04 \leq x \leq 0.11$). *Solid State Communications*, 40(5):629–631, nov 1981.
- [23] T. Ohtani, S. Onoue, and M. Nakahira. Phase relationships and properties in the V-Te system. *Materials research bulletin*, 19(10):1367–1375, 1984.
- [24] Corsin Battaglia, Hervé Cercellier, Florian Clerc, Laurent Despont, Michael Gunnar Garnier, Christian Koitzsch, Philipp Aebi, Helmuth Berger, László Forró, and Claudia Ambrosch-Draxl. Fermi-surface-induced lattice distortion in NbTe $_2$. *Physical Review B*, 72(19), nov 2005.
- [25] Shoichi Nagata, Tsuyoshi Abe, Shuji Ebisu, Yutaka Ishihara, and Kitomi Tsutsumi. Superconductivity in the metallic layered compound NbTe $_2$. *Journal of Physics and Chemistry of Solids*, 54(8):895–899, aug 1993.
- [26] M. H. Van Maaren and G. M. Schaeffer. Some new superconducting group V^a dichalcogenides. *Physics Letters A*, 24(12):645–646, 1967.
- [27] Hongxiang Chen, Zhilin Li, Liwei Guo, and Xiaolong Chen. Anisotropic magneto-transport and magnetic properties of low-temperature phase of TaTe $_2$. *EPL (Europhysics Letters)*, 117(2):27009, jan 2017.
- [28] Chen Chen, Heung-Sik Kim, Alemayehu S. Admasu, Sang-Wook Cheong, Kristjan Haule, David Vanderbilt, and Weida Wu. Trimer bonding states on the surface of the transition-metal dichalcogenide TaTe $_2$. *Physical Review B*, 98(19), nov 2018.
- [29] Y. Liu, W. J. Lu, D. F. Shao, L. Zu, X. C. Kan, W. H. Song, and Y. P. Sun. Structural, electrical, and thermoelectric properties of distorted 1T-Ta $_{1-x}$ Nb $_x$ Te $_2$ single crystals. *EPL (Europhysics Letters)*, 109(1):17003, jan 2015.
- [30] A. H. Thompson and B. G. Silbernagel. Magnetic properties of VSe $_2$: Inferences from the study of metal-rich $V_{1+\delta}$ Se $_2$ compounds. *Journal of Applied Physics*, 49(3):1477–1479, mar 1978.
- [31] L. F. Schneemeyer and M. J. Sienko. The effect of niobium substitution on charge density wave anomalies in vanadium diselenide. *Journal of the Less Common Metals*, 62:343–348, nov 1978.
- [32] A. H. Thompson and B. G. Silbernagel. Correlated magnetic and transport properties in the charge-density-wave states of VSe $_2$. *Physical Review B*, 19(7):3420–3426, apr 1979.
- [33] Juhi Pandey and Ajay Soni. Electron-phonon interactions and two-phonon modes associated with charge density wave in single crystalline 1T-VSe $_2$. *Physical Review Research*, 2(3), jul 2020.
- [34] T. Valla, A. V. Fedorov, P. D. Johnson, P. A. Glans, C. McGuinness, K. E. Smith, E. Y. Andrei, and H. Berger. Quasiparticle Spectra, Charge-Density Waves, Superconductivity, and Electron-Phonon Coupling in 2H- NbSe $_2$. *Physical review letters*, 92(8):086401, 2004.

- [35] F. J. Di Salvo, J. A. Wilson, B. G. Bagley, and J. V. Waszczak. Effects of doping on charge-density waves in layer compounds. *Physical Review B*, 12(6):2220, 1975.
- [36] F. Borsa, D. R. Torgeson, and H. R. Shanks. Charge-density wave amplitudes in $2H - NbSe_2$ and $2H - TaSe_2$ determined by ^{77}Se NMR. *Phys. Rev. B*, 15:4576–4579, May 1977.
- [37] T. Tsuda, H. Yasuoka, Y. Kitaoka, and F. J. Di Salvo. ^{51}V NMR study of the phase transition in $1T-VS_2$. *Journal of Magnetism and Magnetic Materials*, 31:1101–1102, 1983.
- [38] Xu Sun, Tao Yao, Zhenpeng Hu, Yuqiao Guo, Qinghua Liu, Shiqiang Wei, and Changzheng Wu. In situ unravelling structural modulation across the charge-density-wave transition in vanadium disulfide. *Physical Chemistry Chemical Physics*, 17(20):13333–13339, 2015.
- [39] M. Leroux, M. Le Tacon, M. Calandra, L. Cario, M.-A. Méasson, P. Diener, E. Borrisenko, A. Bosak, and P. Rodière. Anharmonic suppression of charge density waves in $2H-NbS_2$. *Physical Review B*, 86:155125, Oct 2012.
- [40] Y. D. Wang, W. L. Yao, Z. M. Xin, T. T. Han, Z. G. Wang, L. Chen, C. Cai, Yuan Li, and Y. Zhang. Band insulator to Mott insulator transition in $1T-TaS_2$. *Nature communications*, 11(1):1–7, 2020.
- [41] Jaydeep Joshi, Heather M. Hill, Sugata Chowdhury, Christos D. Malliakas, Francesca Tavazza, Utpal Chatterjee, Angela R. Hight Walker, and Patrick M. Vora. Short-range charge density wave order in $2H-TaS_2$. *Physical Review B*, 99(24):245144, 2019.
- [42] Xiabin Ding, Jie Xing, Gang Li, Luis Balicas, Krzysztof Gofryk, and Hai-Hu Wen. Crossover from Kondo to Fermi-liquid behavior induced by high magnetic field in $1T-VTe_2$ single crystals. *Physical Review B*, 103(12), mar 2021.
- [43] Sourabh Barua, M. Ciomaga Hatnean, M. R. Lees, and G. Balakrishnan. Signatures of the Kondo effect in VSe_2 . *Scientific Reports*, 7(1), sep 2017.
- [44] Qiang Cao, Frank F. Yun, Lina Sang, Feixiang Xiang, Guolei Liu, and Xiaolin Wang. Defect introduced paramagnetism and weak localization in two-dimensional metal VSe_2 . *Nanotechnology*, 28(47):475703, oct 2017.
- [45] H. N. S. Lee, M. Garcia, H. McKinzie, and A. Wold. The low-temperature electrical and magnetic properties of $TaSe_2$ and $NbSe_2$. *Journal of Solid State Chemistry*, 1(2):190–194, 1970.
- [46] Akio Furukawa, Yoshihide Kimishima, Yasukage Oda, Hiroshi Nagano, and Yoshichika Ōnuki. Magnetic behavior of $1T-TaS_2$ in the Anderson localized state. *Journal of the Physical Society of Japan*, 54(11):4300–4305, 1985.
- [47] Hongtao Liu, Yunzhou Xue, Jin-An Shi, Roger A. Guzman, Panpan Zhang, Zhang Zhou, Yangu He, Ce Bian, Liangmei Wu, Ruisong Ma, Jiancui Chen, Jiahao Yan, Haitao Yang, Cheng-Min Shen, Wu Zhou, Lihong Bao, and Hong-Jun Gao. Observation of the Kondo Effect in Multilayer Single-Crystalline VTe_2 Nanoplates. *Nano Letters*, 19(12):8572–8580, nov 2019.
- [48] Charles Kittel. *Introduction to solid state physics*. John Wiley & sons, inc, 2005.
- [49] H. SCHÄFER. Chemical Transport Processes as an Aid in Preparative Chemistry. Combination of Transport Reactions with Other Processes. In *Chemical Transport Reactions*, pages 115–131. Elsevier, 1964.
- [50] G. A. Wiegers. Physical properties of first-row transition metal dichalcogenides and their intercalates. *Physica B+C*, 99(1-4):151–165, jan 1980.
- [51] D. R. Hamann. New Solution for Exchange Scattering in Dilute Alloys. *Phys. Rev.*, 158:570–580, Jun 1967.
- [52] Kei Yosida. Anomalous Electrical Resistivity and Magnetoresistance Due to an $s - d$ Interaction in Cu-Mn Alloys. *Phys. Rev.*, 107:396–403, Jul 1957.
- [53] Tsuyoshi Sekitani, Michio Naito, and Noboru Miura. Kondo effect in underdoped n-type superconductors. *Phys. Rev. B*, 67:174503, May 2003.
- [54] K. Park, L. S. Wu, Y. Janssen, M. S. Kim, C. Marques, and M. C. Aronson. Field-tuned Fermi liquid in quantum critical YFe_2Al_{10} . *Phys. Rev. B*, 84:094425, Sep 2011.
- [55] Hui Pan. Magnetic and Electronic Evolutions of Hydrogenated VTe_2 Monolayer under Tension. *Scientific Reports*, 4(1), dec 2014.
- [56] Huei-Ru Fuh, Ching-Ray Chang, Yin-Kuo Wang, Richard F. L. Evans, Roy W. Chantrell, and Horng-Tay Jeng. Newtype single-layer magnetic semiconductor in transition-metal dichalcogenides VX_2 ($X=S, Se$ and Te). *Scientific Reports*, 6(1), sep 2016.
- [57] C. J. Sayers, L. S. Farrar, S. J. Bending, M. Cattelan, A. J. H. Jones, N. A. Fox, G. Kociok-Köhn, K. Koshmak, J. Laverock, L. Pasquali, and E. Da Como. Correlation between crystal purity and the charge density wave in $1T-VSe_2$. *Physical Review Materials*, 4(2), feb 2020.

- [58] A. O. Fumega, M. Gobbi, P. Dreher, and W. Wan et al. Absence of Ferromagnetism in VSe_2 Caused by Its Charge Density Wave Phase. *The Journal of Physical Chemistry C*, 123(45):27802–27810, oct 2019.
- [59] Akira Toriumi and Shoji Tanaka. Galvanomagnetic properties of 1T- VSe_2 . *Physica B+C*, 105(1-3):141–145, may 1981.
- [60] C. F. van Bruggen and C. Haas. Magnetic susceptibility and electrical properties of VSe_2 single crystals. *Solid State Communications*, 20(3):251–254, oct 1976.
- [61] Michel Bayard and M. J. Sienko. Anomalous electrical and magnetic properties of vanadium diselenide. *Journal of Solid State Chemistry*, 19(4):325–329, dec 1976.
- [62] S. Kondo, D. C. Johnston, and L. L. Miller. Synthesis, characterization, and magnetic susceptibility of the heavy-fermion transition-metal oxide LiV_2O_4 . *Physical Review B*, 59:2609–2626, Jan 1999.
- [63] Manuel Bonilla, Sadhu Kolekar, Yujing Ma, Horacio Coy Diaz, Vijaysankar Kalappattil, Raja Das, Tatiana Eggers, Humberto R. Gutierrez, Manh-Huong Phan, and Matthias Batzill. Strong room-temperature ferromagnetism in VSe_2 monolayers on van der Waals substrates. *Nature Nanotechnology*, 13(4):289–293, feb 2018.
- [64] Jiyong Yang, Weike Wang, Yan Liu, Haifeng Du, Wei Ning, Guolin Zheng, Chiming Jin, Yuyan Han, Ning Wang, Zhaorong Yang, Mingliang Tian, and Yuheng Zhang. Thickness dependence of the charge-density-wave transition temperature in VSe_2 . *Applied Physics Letters*, 105(6):063109, aug 2014.